AIAA 2002-4269

An Experimental Study of a Pulsed Electromagnetic Plasma Accelerator

Y. C. Francis Thio[1], R. Eskridge[1], M. Lee[1], J. Smith[1], A. Martin[1], T. E. Markusic[1], Jason T. Cassibry[2]

(1) George C. Marshall Spaceflight Center
(2) University of Alabama in Huntsville.

38th AIAA/ASME/SAE/ASEE Joint Propulsion Conference & Exhibit
7-10 July 2002
Indianapolis, IN

AIAA-2002-4269

An Experimental Study of a Pulsed Electromagnetic Plasma Accelerator

Y. C. Francis Thio, R. Eskridge, M. Lee, J. Smith, A. Martin, T. E. Markusic, Jason T. Cassibry[1]
NASA Marshall Space Flight Center

Abstract

Experiments are being performed on the NASA Marshall Space Flight Center (MSFC) pulsed electromagnetic plasma accelerator (PEPA-0). Data produced from the experiments provide an opportunity to further understand the plasma dynamics in these thrusters via detailed computational modeling. The detailed and accurate understanding of the plasma dynamics in these devices holds the key towards extending their capabilities in a number of applications, including their applications as high power (> 1 MW) thrusters, and their use for producing high-velocity, uniform plasma jets for experimental purposes. For this study, the 2-D MHD modeling code, MACH2, is used to provide detailed interpretation of the experimental data. At the same time, a 0-D physics model of the plasma initial phase is developed to guide our 2-D modeling studies.

1 Introduction

In this paper, we describe an experimental study in progress of a pulsed plasma accelerator at NASA Marshall Space Flight Center. The study was done in the context of developing a pulsed plasma accelerator as a driver for magnetized target fusion (MTF). In plasma jets driven MTF, a magnetized plasma (designated as the target) is compressed inertially by a plasma shell formed by the merging of a spherical array of plasma jets[(1)]. In the near term, a physics exploratory experiment (PLX)[(2)] consists of using twelve plasma guns arranged in a circle, launching plasma jets towards the center of a vacuum chamber, Fig. 1. The velocity of the plasma jets required for the exploratory experiment is 200 km/s, and each jet is to carry a mass of 0.2 mg – 0.4 mg. A candidate plasma accelerator for launching these jets consists of a coaxial plasma gun of the Marshall type and is given the name PEPA-1 (Pulsed Electromagnetic Plasma Accelerator) which is described in a companion paper[(3)].

The Marshall gun is a plasma accelerator consisting of a pair of coaxial cylindrical electrodes. Current from a capacitor bank enters at one of the electrodes, crossing the gap between the electrodes through a plasma, and returns to the capacitor bank via the other electrode. The current following in the electrodes generates an azimuthal magnetic field in the region between the electrodes. This magnetic field acts on the plasma current to produce the electromagnetic $\mathbf{j} \times \mathbf{B}$ (Lorentz) force on the plasma, accelerating the plasma down the tube. In a real device, the PPT displays a wide range of complexity in the plasma behavior.

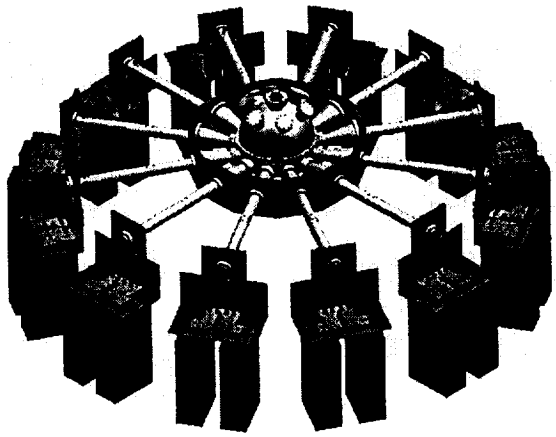

Figure 1. The Plasma Liner Physics Exploratory Experiment (PLX), consisting of merging 12 plasma jets launched by 12 coaxial plasma guns.

At the NASA Marshall Space Flight Center, a new pulsed power laboratory, Fig. 2, has been developed to undertake research of transient processes occurring in high energy density plasmas. Developing the experimental infrastructure of the laboratory involves the development and testing of the pulsed power supply (a capacitor bank) and its transmission manifold, the high-voltage charging power supply, the control and firing subsystem, a fast and low-jitter trigger generator, the multi-channel data acquisition system and the plasma diagnostics. A pulsed plasma device serving as an electrical load as well as a switch for the testing and commissioning of the pulsed power experimental system is required. Since the immediate application of the pulsed power laboratory is to conduct research in support of magnetized target fusion propulsion driven by high-velocity plasma guns[(2)], a device involving plasma

[1] University of Alabama, Huntsville, USA.

acceleration of some kind would be useful as an electrical load for the test. The result was a coaxial plasma acceleration device that was given the name PEPA-0 as a precursor to our principal research accelerator, PEPA-1.

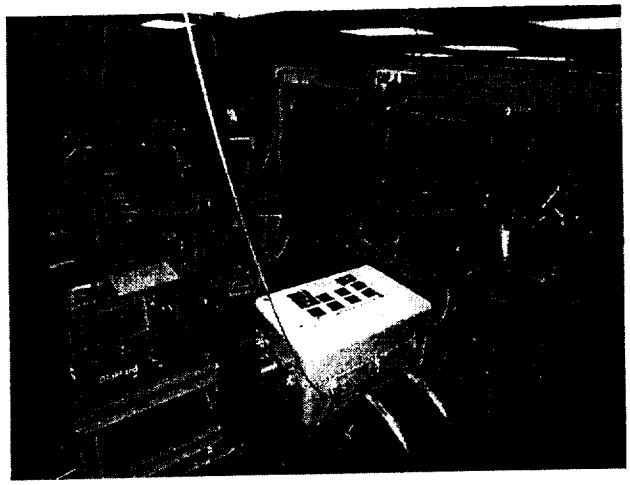

Figure 2. The new pulsed power laboratory at NASA Marshall Space Flight Center.

Nevertheless, the working of the plasma gun is similar to a pulsed plasma thruster, and thus provided an opportunity for studying the plasma dynamics in a coaxial pulsed plasma thruster. In particular, it provides the opportunity of benchmarking our computer models against experimental data. It has become a rather useful device that aids in the design of our principal research accelerator (PEPA-1), besides serving an electrical load for the development of the experimental infrastructure. As a design tool for PEPA-1, we are in the process of adding and testing other features on this gun that we plan to incorporate in PEPA-1.

2 The Experimental System and the Diagnostics

PEPA-0 consists of a pair of coaxial cylindrical electrodes. The inner electrode has a diameter of 2.667 cm (1.05 in.) and is 0.4635 m (18.25 in.) long measured from the breech plug, Fig. 3. The outer electrode has a diameter of 5.398 cm (2.125 in.) and is 0.8128 m long measured from the same breech plug. The plasma gun is connected directly to a pair of capacitors of 330 μF each, via a pair of transmission plates with a total inductance estimated at 230 nH without the use of any external switches, Figure 4. The capacitors are rated for 10 kV maximum voltage, though experiments to-date have been conducted with voltage below 6 kV.

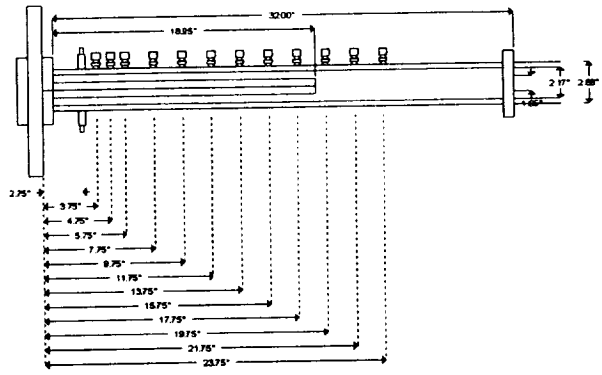

Figure 3. The experimental device (PEPA-0), consisting of a pair of coaxial cylindrical electrodes.

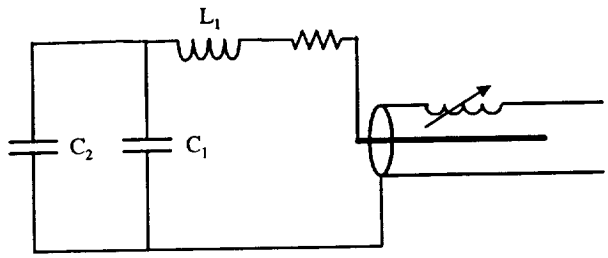

Figure 4. Circuit diagram for PEPA-0. ($C_1 = C_2 =$ 320 mF, max. voltage: 5 kV, Total stored energy: 8 kJ, L_1 =214 nH)

At 6.985 cm (2.75 in.) from the breech plug is a set of six ordinary automobile spark plugs. The bent tip of the outer spark terminal is clipped flushed with the outer casing, so that the spark plug has the geometry of a miniature coaxial plasma gun. The spark plugs are inserted into the outer electrode of the main accelerator through Swedgelok fasteners. These spark plugs are used for initiating the capacitive discharge.

The plasma gun is physically connected and sealed to a hemispherical vacuum chamber Fig. 5. The vacuum chamber is equipped with a number of diagnostic ports. One port is used for taking high-speed photograph of the plasma jet launched from the thruster. One port is used for making optical emission spectroscopy. One port is used for a set of five light pipes focused at points in the chamber along the axis of the plasma thruster. These light pipes are used to measure the velocity of the plasma jet as it travels through the central portion of the chamber.

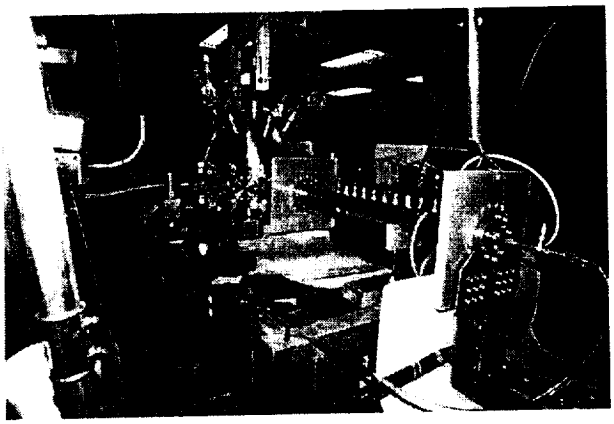

Figure 5. The experimental system showing the pulsed plasma thruster connected to a hemispherical vacuum chamber. The vacuum chamber and the length of the plasma thruster is equipped with a number of diagnostics ports.

The gun is equipped with a number of diagnostic ports (holes) along its length, Figure 6. They have been used for holding light pipes and magnetic (bdot) probes. One set of ports are used for laser interferometry for electron density measurements. A set of six light pipes for in-bore optical emission monitoring and five magnetic probes were used in the series of tests just completed.

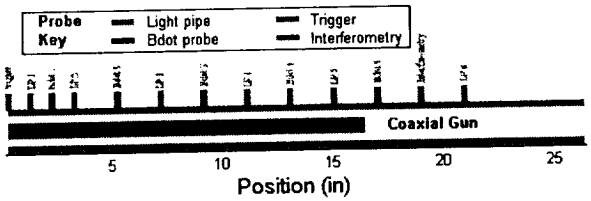

Figure 6. Diagnostics on PEPA-0.

The exterior diagnostics (in the vacuum chamber) are planned to be reported elsewhere. In this paper we shall report and analyse the mainly in-bore measurements taken with the magnetic probes and light pipe.

2.1 Light Pipes

A set of seven light pipes were used to determine the position and time of the radiating plasma jet as it passed through the gun and into the chamber. The first six of these light pipes were stationed along the length of the gun. LP10 was located downstream of the gun in a velocimeter in the chamber. LP10 was positioned to view a fixed point approximately 30 cm downstream of LP8, the light pipe positioned closest to the coaxial gun muzzle. Table 1 gives the positions of each probe in inches.

Probe Name	Position (in)
LP1	1.0
LP2	3.0
LP3	7.0
LP4	11.0
LP5	15.0
LP8	21.0
LP10	52.0

Table 1. Positions of the light pipe probes as measured from the trigger.

Each light pipe consisted of a collimator holding the end of an 10 yard long ESKA plastic fiber. Each collimator was constructed by wrapping a 6 cm long, brown stirring straw with a 35 mm length of 1 mil Kapton tape. The tape built up the diameter of the straw to make a snug fit inside a 5.7 cm long quartz tube. The tube was inserted into a ¼" pipe to swage male connecter, which was screwed into the gun barrel. The fiber was terminated to a 16 channel H6568 Hamamatsu Photonics photomultiplier tube (PMT). The PMT was common to all light pipes. A 10 channel DC240 2.0 Gigasample Acqiris data acquisition system temporarily stored the raw signal which was downloaded to a computer.

2.2 Magnetic Field Probes

A set of five B-dot probes were positioned along the gun in the outer electrode as given in Table 2. The probes were positioned 3-4 inches apart, beginning with 1 inch from the trigger for $\dot{B}_{1\theta}$.

Probe Name	Position (in)
$\dot{B}_{1\theta}$	2.0
$\dot{B}_{2\theta}$	5.0
$\dot{B}_{3\theta}$	9.0
$\dot{B}_{5\theta}$	13.0
$\dot{B}_{6\theta}$	17.0

Table 2. Positions of the bdot probes as measured from the trigger.

A simple schematic of one of the bdot probes is shown below in Figure 7. The probes were designed to measure the θ component of the magnetic field. Each probe was made with a T-shaped piece of fiber glass with approximate dimensions, Fig. 7. A pair of holes were drilled near the bottom of the 'T' for the coils. #40 gauge magnetic wire was wound around the section between the holes as shown. The probes had between 13-21 turns. As many turns as physically possible were

wound for probe sensitivity, at the expense of frequency response. The leads from the coil were tightly twisted to minimize stray magnetic field pickup, and glued to the side of the probe along its length. The ends were soldered to a pair of M17-119 RG 174 wires shielded by a metal braid. The fiber glass stock was then wrapped with Kapton, and the probe was inserted into a quartz tube. The tube was inserted into a ¼" pipe to swage male connecter, which was screwed into the gun barrel. The quartz tube was at a position such that the coil center was .025 meters from the center electrode axis. This placed the top edge of the coil about 0.25 mm below the inner surface of the outer electrode.

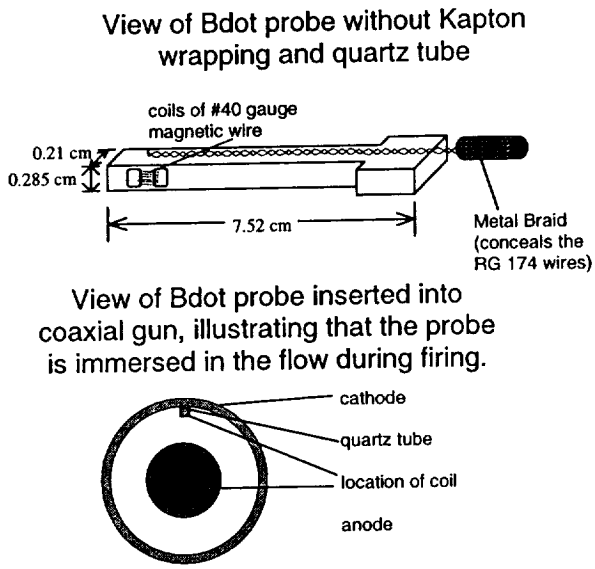

Figure 7. Sketch of a bdot probe and probe location in the plasma accelerator

The calibration factor can be estimated with Faraday's law,

$$\nabla \times E = -\frac{\partial B}{\partial t}$$

where E is the electric field and B is the magnetic field. Using Stokes theorem, we can show $\oint E \cdot dl = -\frac{\partial \phi}{\partial t}$ where ϕ is the total magnetic flux through a loop, and the contour integral of E around the coils is the voltage, $\oint E \cdot dl = v$. The magnetic flux is given by $\phi = BnA$, where n is the number of turns in the coil, and A is the cross sectional area. The voltage is the signal measured across the leads of the probe, assuming the frequency is lower than the cutoff frequency of the probe. The magnetic field seen by the coils in the probe is assumed to be due to the current of the inner conductor, so that

$$B = B_\theta = \frac{\mu_0 I}{2\pi r}$$

where I is the current and r is the distance measured from the axis of symmetry within the center conductor. Thus, the current is calculated with

$$I = -K \int_0^t v d\tau$$

where K is the calibration factor given by

$$K = -\frac{2\pi r}{\mu_0 n A}$$

This result should give the correct calibration factor to within 10%. The larger the number of turns and greater cross sectional area, the lower the uncertainty in the calculation. A more precise calibration method requires measuring the bdot probe voltage when the probe is inserted into a known pulsed field. This was accomplished by shorting the gun at the muzzle end with the capacitor bank charged, and measuring the current with a Pearson coil. A Rogowski coil was also calibrated during this procedure and is discussed below.

2.3 Rogowski Coil

For measurement of the current at the capacitor, a Rogowski belt was constructed with 200 turns of Beldin 26 AWG magnetic wire would around a 20 cm length of the center core of a RG58 cable. The coaxial cable was stripped of its outer conductor. One lead from the magnetic wire was soldered to the center conductor. The cross sectional area of the coil was approximately 1.14 m^2. The calibration factor can be calculated with the equation above for K, with $2\pi r$ equaling the length of the coil in meters. The Bdot probes and Rogowski coil have been calibrated, and the calibration factor has been compared with the theoretical results as shown in Table 3.

Probe	r (m)	n	Coil Area (m^2)	Calibration Factor	
1	0.025	10	3.15×10^{-6}	4.85×10^{5}	3.10×10^{5}
2	0.025	20	3.15×10^{-6}	4.85×10^{5}	2.60×10^{5}
4	0.025	10	3.6×10^{-6}	4.24×10^{5}	2.75×10^{5}
5	0.025	20	3.41×10^{-6}	4.48×10^{5}	2.35×10^{5}
6	0.025	10	3.23×10^{-6}	4.73×10^{5}	2.70×10^{5}
Rogowski	0.03183	200	1.14×10^{-5}	6.98×10^{4}	7.25×10^{4}

Table 3. Summary of the calibration results for the bdot and Rogowski magnetic field probes.

2.4 Photography

Images were taken with a PI Max gated camera with 10 nanosecond exposure, and a Cordin camera capable of taking 8 exposures at a rate of 1 Ghz.

3 Experimental Results

B-dot and light pipe probes were among the diagnostics used in the series of experiments with PEPA-0. The probe stations are as shown in Fig. 6. A typical light pipe probe signal is shown in Fig. 8. A sharp rise in the signal indicates that a high temperature plasma is within the field of view of the probe. Because of some electrical problem with the photomultiplier tubes, the intensity of the signal does not necessarily correlate to the intensity of the signal. This problem is under investigation.

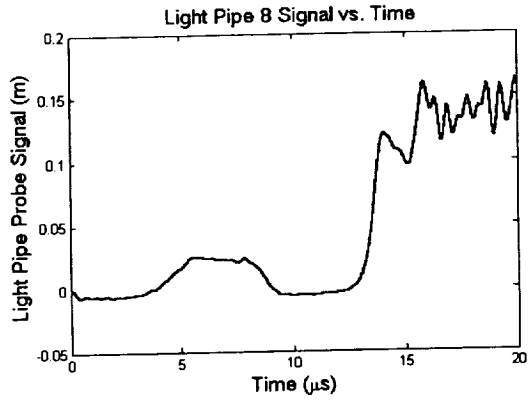

Figure 8. A typical light pipe probe signal.

The integrated signal for $B_{1\theta}$, the probe closest to the trigger, is given for a typical shot, Fig. 9. Figure 9 shows the current rises sharply from about 1 μs and peaks around 18 μs at about 155 kAmps. Figure 10 shows scaled bdot probe currents as a function of position. This chart clearly indicates a current sheet propagating downstream. The run number is given for reference.

From Fig. 10 one can estimate the velocity by dividing the distance between adjacent probes by time to a fraction of probe current peak. Table 4 below is a calculation of velocity vs. bdot probe position for 10% of the peak current for each probe. The exit velocity of the gun is about 41 km/s. As a consistency check, one can repeat this calculation for the light pipe signals. Table 5 below is a summary of velocity vs. position for 10% of the peak light pipe signals. The exit velocity calculated from the light pipe probes is about 53 km/s, which is in fairly good agreement with the Bdot probe data.

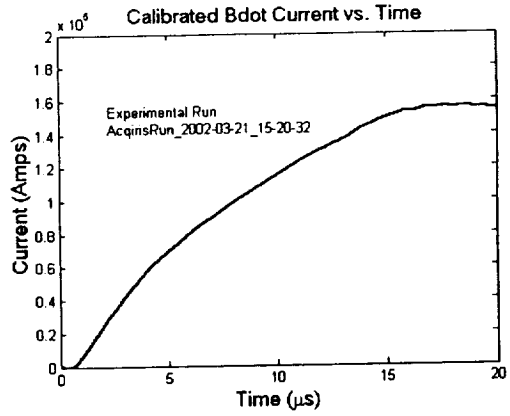

Figure 9. Current from the bdot probe $B_{1\theta}$, showing the current in the vicinity of the gun breech.

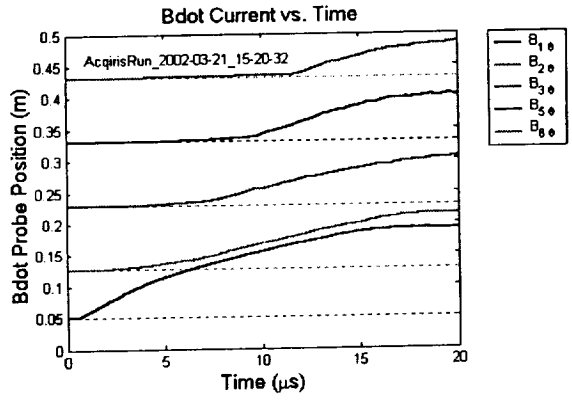

Figure 10. Bdot probe current as a function position along the coaxial gun.

Probe	Time (μs)	Velocity (m/s)
$B_{1\theta}$	1.55	32774.19
$B_{2\theta}$	5.05	52551.72
$B_{3\theta}$	7.38	29028.57
$B_{5\theta}$	9.81	43605.15
$B_{6\theta}$	12.07	41810.7

Table 4. Velocity calculated between adjacent bdot probes by dividing relative probe position by relative time to 10% of peak signal.

Probe	Time (μs)	Velocity (m/s)
LP1	1.39	18273.38
LP2	4.24	39379.84
LP3	6.36	35649.12
LP4	7.82	47924.53
LP5	10.68	69589.04
LP8	13.15	53286.71

Table 5. Velocity calculated between adjacent light pipe probes by dividing relative probe position by relative time to 10% of peak signal.

The performance of PEPA-0 was so repeatable that an animation was created from a series of consecutive shots by simply changing the delay time between the trigger pulse and the exposure on the camera. Two frames from this animation are shown in Fig. 11. Each frame was taken with a PI Max gated camera with 10 nanosecond exposure. The velocity estimated from these shots is about 50 to 60 km/s.

Figure 11. Images of the plasma jet propagating through the vacuum chamber taken with the PI Max camera. PEPA-0 was so repeatable that an animation could be made from photos of consecutive shots, changing the delay time between the trigger pulse and the exposure (usually 0.5 μs increments).

The Cordin camera is capable of taking 8 photos at a rate of 1 billion frames per second. For the PEPA-0 experiments, the lense was focused on the muzzle end of the gun from the opposing port on the vacuum chamber. Images from the Cordin camera are shown in Fig. 12, showing a bright ring propagating down the chamber.

4 Modeling the Experiment

Detailed magneto-plasma dynamic modeling provides the means to understand this complexity, and hence to improve its performance. Despite the fact that research and development of pulsed plasma thrusters has been conducted for more than 40 years[4-6], magnetohydrodynamic (MHD) modeling using two or more spatial dimensions to analyze the detailed plasmadynamic behavior of pulsed plasma thrusters and comparing the modeling results with experiments has been few and far between. The work of Keefer[7] involving the use of a sophisticated MHD code such as MACH2[8] to the modeling of plasma thrusters is a relatively recent event. Mikellides has applied the code to model related but very different devices, the MPD thrusters[9-13]. A recent study was made by Shen and co-workers[14]. Sankaran is developing a new 2-D MHD code for modeling MHD flows in similar thrusters[15]. Earlier work includes those of Andrenucci[16] and Ao [17].

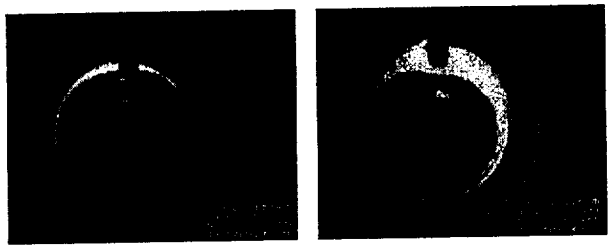

Figure 12. Images of the plasma accelerating down barrel of PEPA-0 taken with the Cordin camera.

Our principal tool for modeling and interpreting the experimental results is the 2-D MHD code MACH2 developed by the US Air Force Research Laboratory (Ref). In our experience of running MACH2 so far, we have found that the correct specification of the initial condition of the plasma is singularly the most important factor in getting good agreement between the computational results and the experiment. To set up the initial conditions correctly, we need to examine the plasma initiation phase in the experiment and develop an appropriate physics model for this phase of the evolution of the plasma up to the point where MHD assumptions become appropriate. In PEPA-0, the plasma initiation phase was dominated by particle kinetic effects.

4.1 The Plasma Initiation Phase

More than a hundred shots have been taken with PEPA-0. One characteristic of the experimental system is that it has been very reliable and its performance is very reproducible. Essentially identical experimental results are obtained with identical charging voltages on the capacitors.

We will select one of the more recent test shots for a detailed discussion. This shot was labeled Shot 2002-03-21_15-20-32. In this shot, the thruster was prefilled with He at a pressure of 8.5 ± 0.5 mTorr (~ 1.1 Pa) with

0.46% Ar. The part of the breech between the outer and inner electrode exposed to the plasma is a Teflon insulator for this shot. The capacitor is charged to a voltage of 5.36 ± 0.2 kV. The capacitive discharge was initiated by a sharp pulse (~ 5 ns) of current (~ 300 A) and voltage (~ 30 kV) to each of the six modified spark plugs. The modified spark plugs function as miniature coaxial plasma guns ejecting a high-velocity stream of charged particles. The energetic electrons and the associated UV radiation further ionize the He gas in the gun bore. As the electrodes are subjected to the high charging voltage, a Townsend avalanche occurs and turns on the main current pulse. In this shot the current reaches a peak of 155 kA at a time of 18 μs, as measured by the first bdot probe placed near the breech, Fig. 9.

Assume an initial temperature of 25 ^{o}C for the pre-filled helium gas, its particle density is estimated as 2.8×10^{20} m^{-3}. According to Kaye and Laby[18], the effective molecular radius of helium for a classical estimate of the molecular mean free path is 2.18×10^{-10} m. According to Chapman and Cowling[19], a classical estimate of the molecular mean free path is,

$$\lambda = \frac{1}{\sqrt{2}} \frac{1}{n\pi r_m^2},$$

where r_m is the classical molecular radius and n is the particle number density. For above set of parameters, the molecular mean free path in the pre-filled helium gas is estimated to be 1.7 cm, relatively large in terms of the dimension of our plasma thruster.

In 50 ns, the current rises rapidly to about 0.7 kA, producing a magnetic pressure of 40 Pa at the mid point between the electrodes. This pressure is about 40 times greater than the in-bore gas pressure, sufficient to produce a shock wave through the pre-filled gas.

We argue that this shock cannot be collisional in nature, that is it cannot be a hydrodynamic or a collisional hydromagnetic shock wave. For these collisional shock waves, the density of the gas can at most increases by a factor of $(\gamma + 1)/(\gamma - 1)$ or 4 for $\gamma = 5/3$. The magnetic pressure can be balanced by this gas density if the temperature of the gas goes to approximately 0.3 eV. The temperature is not sufficient to produce any significant ionization. Thus for a collisional shock, the pertinent mean free path in determining the thickness and structure of the shock front is that of the neutral particles. As we have seen above, the neutral mean free path is about 1.7 cm and a typical hydrodynamic shock front has a thickness of several (~ 10 times) the mean free path, making the shock front rather broad, about 17 cm.

We conclude that, up to about 50 ns, the shock produced must be of a collisionless magnetic kind. In the case of a collisionless shock, steep gradients of the magnetic field occurs over distances much shorter than the particles mean free path, where large electrical current flows producing the shock. The collisionless shock front is the region through which the initial current flows. In this collisionless shock the density remains more or less constant at the value of the background gas. The shock travels at about 40 km/s. In 50 ns, the front spread to about 2 mm (<< 1.7 cm). The current density is of the order of 1 MA/m^2 and, to balance the magnetic pressure, the corresponding gas temperature needs to be about 10 eV, sufficiently high to produce ionization. Strictly, the concept of temperature is not appropriate here as the plasma is highly non-equilibrium and non-Maxwellian up to this point. We borrow the concept of temperature loosely to indicate the trend of the discussion. The speed at which the Hall current propagates is of the same order as the collisionless shock, about 40 km/s. The plasma dynamic during this phase is highly dominated by particle kinetics. MHD models would not be appropriate during this regime.

The scenario changes rapidly in the next 50 ns. At 100 ns, the current reaches a value of 1.4 kA, the magnetic pressure at the mid-point between the electrodes is now 160 Pa. This pressure is 160 times and is large enough to sustain a collisional hydrodynamic shock temperature of more than 1 eV, even if the density increases by a factor 4 over the background gas. At this temperature, sufficient degree of ionization can be sustained, whereby the ion-ion collisions and their mean free paths come into play. At this density and temperature, the ion-ion mean free path is of the order of 1 mm, sufficiently smaller than the thickness of a collisionless shock. The thickness of a collisional shock here (an MHD shock in this case as the shock is dominated by the magnetic pressure and the ion-ion collisions) is about 10 mm (being ~ 10 times the ion-ion mean free path). The collisionless shock front has also spread to about the same extent of ~ 10 mm. Therefore the shock makes a transition from being collisionless to a collisional one.

The corresponding current density is 9×10^5 A/m^2. At this point, a collisional plasma is more or less established. It is then appropriate to proceed with a MHD model for the plasma dynamics. We thus use the conditions deduced from the above 0-D physics reasoning as the initial conditions to start our MACH2 runs to model the experimental results. Specifically, we start the MACH2 run at t = 100 ns, with an initial plasma with the following parameters: The plasma has a

thickness of 1.26 cm, a temperature of 3.665 eV, and a particle density of 2.78×10^{20} m^{-3}.

We note that with time, the current is not limited to the width of the MHD shock front. Rather it will spread subjected to the diffusion of the magnetic field, the diffusivity of which is governed by the plasma resistivity. Using Braginskii's coefficients, the plasma resistivity may be estimated to be ~ 10^{-4} ohm-m. At a time of 500 ns for example, the skin depth for the magnetic field is about 10 mm, whereas the shock front has diminished to less than 1 mm thick.

4.2 The Main Acceleration Phase

The main acceleration phase is modeled using MACH2. MACH2 is a 2 ½D multiblock, Arbitrary Lagrangian Eulerian (ALE), resistive magnetohydrodynamic (MHD) code that carries all three spatial components of vectors, but allows no quantity to depend on the coordinate that is normal to the computational plane[20]. MACH2 solves the mass, momentum, electron energy, ion energy, radiation energy density, and magnetic induction equations in a fractional time-split manner for the flow variables. The equations are closed with various equations of state and transport coefficient models. For the results presented here, a new tabular equation of state package, Aurora, was developed and implemented into MACH2. Aurora was designed to calculate the equilibrium thermodynamic quantities of dissociated and ionized polyatomic species, such as Teflon or polyethylene. The details of Aurora are to be discussed elsewhere.

Figure 13 shows the computational domain, along the right hand side of the axis of symmetry. The mirror of the domain is shown for visual reference. The physics in the model include thermal diffusion, magnetic field diffusion, rlc circuit model with 5400 V, 660 μF capacitance, 180 nH external inductance, 1.0 mΩ external resistance, Teflon ablation along lower boundary of the trigger block, as indicated in Fig. 13 below. The domain contained an initial global mass density of 1.5 E-4 kg/m3 with 7.54 E-6 in the trigger block. The initial global temperature was .025 eV (270 K) with 3.665 eV in trigger block.

Comparisons of MACH2 with Experiment

MACH2 was run to simulate PEPA-0 experiments. Virtual bdot probes were set in the MACH2 run in the same positions as in the experiment. The current from $B_{1\theta}$ obtained with MACH2 is overlaid with the current $B_{1\theta}$ in the experiment, Fig. 14. Very good agreement is obtained between the two.

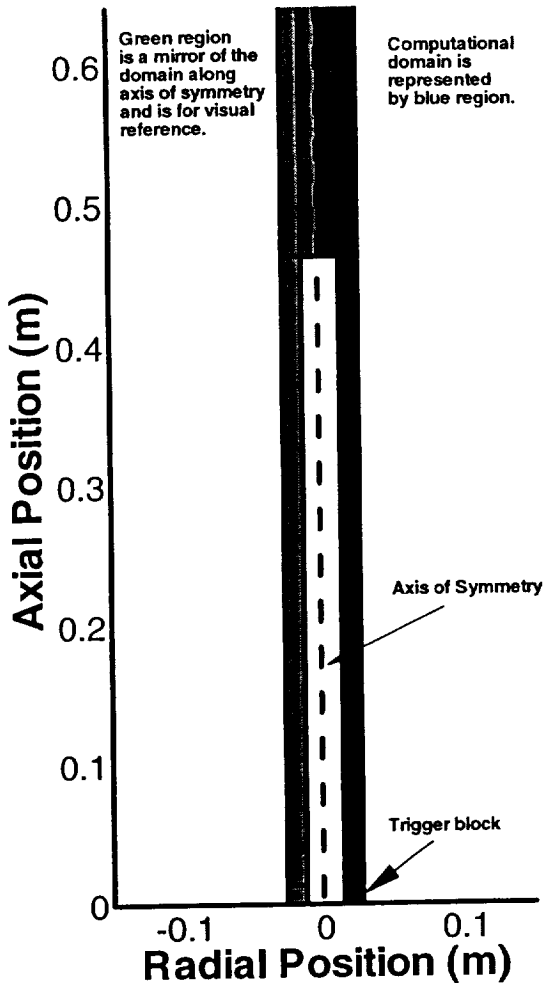

Figure 13. Computational Domain for PEPA-0.

Figure 15 is an overlay of all the probe currents as a function of position. Very good agreement is achieved between the experiment and theory, and is well within the uncertainty in the experimental measurements.

Two Dimensional MACH2 results

Having obtained reasonable agreement of the current as function of position with experiment, we proceed to examine two dimensional plots of some of the plasma properties. The results to follow in this section are vector and contour plots of current, velocity, density, temperature, and pressure, at 7.5 and 15 μs. The aspect ratio has been stretched, compared with Fig. 13, to reveal more detail within the computational domain.

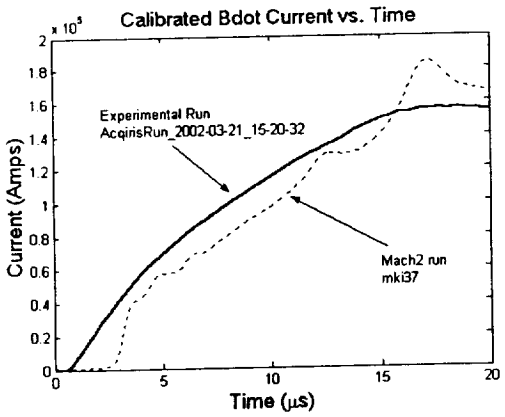

Figure 14. Comparison of Bdot probe data from experiment and MACH2 results.

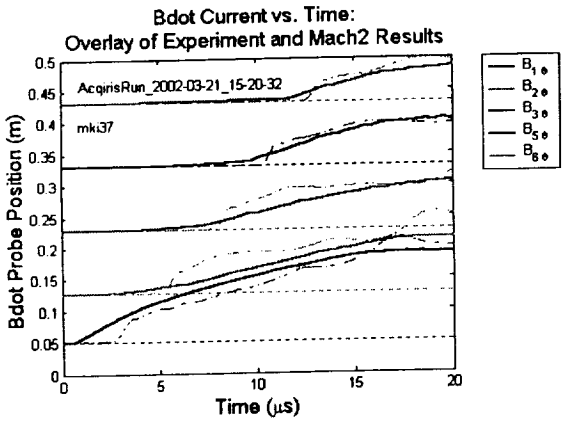

Figure 15. Bdot current as a function of probe position: comparison of experiment and MACH2 results.

Figure 16 shows the propagation of the current sheet, along with the corresponding velocity of the fluid. The radial component of the current density dominates, as indicated by the direction of the vectors in the right half of each plot. Towards the leading edge of the current sheet, the velocity displays a wide range in value, from 75 km/s at the anode to about 20 km/s near the cathode. A simple dz/dt calculation of the current sheet velocity estimates that the bulk motion of the plasma is about 40 km/s, which is consistent with the velocities determined from the bdot probe and light pipe data.

A sizeable amount of material is accelerated with the current sheet, Figure 17. The leading edge of the current sheet consists of a relatively high density front. Following constant lines of density, the material front towards the anode leads the material near the cathode, Fig. 17. Comparison with Fig. 16 shows the same trend with lines of constant velocity. Island-like regions of high pressure are seen in Fig. 17 which correspond with regions of high density along the cathode. These high pressure, high density islands are entrained with the current sheet. Careful comparison of the current contour and vector plot in Fig. 16 with the pressure contours at 15 μs illustrates that the current flows in regions of strong pressure gradients consistent with the fact that the bulk of the plasma current is a manifestation of the diamagnetic drift.

The leading edge of the current sheet hovers between 0.5 and 2eV, Fig. 18. The temperature contours tend to follow the current diffusion, since the main heating mechanism is ohmic dissipation. Although some local hot spots can be as high as 15 eV (probably numerical artifacts), the plasma typically does not exceed 4 eV. It should be mentioned that radiation is not turned on in the model, as the opacities have not been added to the Aurora equation of state package. It is expected that this temperature will be lower once the radiation is accounted for.

4.3 0-D Modeling Results

A 0-D code based on an arbitrary combination of the 'slug' and 'snowplow' models has been developed to assist in the modeling efforts of higher order codes such as MACH2. It is believed that much of the material entrained in the current sheet is from the electrode erosion off the anode and cathode. This is based on the author's experience. It is further evidenced by the simple observation of metallic material deposited on the vacuum port directly downstream of the muzzle of PEPA-0, following a series of shots. An electrode erosion model based on Coulomb transfer ablation was added to the 0-D code, and the ablation rate was adjusted until the plasma jet reached the position of light pipe 8, near the exit of the gun barrel. The resulting ablation rate was 104 μg/Coulomb, which gave a mass of 0.15 mg eroded from the wall. This is in agreement with MACH2, which gives a plasma jet mass of approximately 0.1 mg of material traveling 40 km/s or faster. The exit velocity from the 0-D code was 50 km/s, in agreement with the experimental and computational results. An electrode erosion model is to be implemented into MACH2 to study these effects more precisely.

5 Summary

A new, pulsed power laboratory has been established at NASA/Marshall for developing advanced plasma accelerators for application to MTF. A plasma gun test

bed (PEPA-0) has been developed to assist the design and development of the plasma accelerator (PEPA-1) required for PLX. Approximately 0.1 mg of a plasma jet has been launched to ~ 50 km/s. Computational support for the experimental research have been developed. Appropriate physics models have been introduced into the USAF MACH2 2-D MHD code to provide good agreement with experimental results.

References

1. Y.C.F. Thio, E. Panarella, R.C. Kirkpatrick, C.E. Knapp, and F. Wysocki, eds. *Magnetized Target Fusion in a Spheroidal Geometry With Standoff Drivers.* Current Trends in International Fusion Research, A Review. Proceedings of the 2nd Symposium, ed. E. Panarella (NRC Press, National Research Council of Canada, Ottawa, Canada, 1999).
2. Y. C. Francis Thio, C. E. Knapp, R. C. Kirkpatrick, R. E. Siemon, P. J. Turchi, "A Physics Exploratory Experiment on Plasma Liner Formation," *Journal of Fusion Energy*, **20**, 1, (March 2002).
3. Y. C. F. Thio, J. T. Cassibry, T. E. Markusic, "Pulsed Electromagnetic Acceleration of Plasmas," AIAA-2002-3803, 38th AIAA/ASME/SAE/ASEE Joint Propulsion Conference & Exhibit, Indianapolis, IN.
4. J.D. Filliben, Electric Thruster Systems. Report CPTR-97-65., (Chemical Propulsion Information Agency, John Hopkins University, Columbia, MD, USA, 1997), p. 168.
5. R.L. Burton and P.J. Turchi, "Pulsed Plasma Thruster," Journal of Propulsion and Power 14, 716 (1998).
6. P.J. Turchi, "Directions for Improving PPT Performance," International Electric Propulsion Conference (1997, 1997).
7. D. Keefer and R. Rhodes, "Electromagnetic Acceleration in Pulsed Plasma Thrusters," International Electric Propulsion Conference (1997, 1997).
8. R.E.J. Peterkin, J.H. Degnan, T.W. Hussey, N.F. Roderick, and P.J. Turchi, "A Long Conduction Time Compact Torus Plasma Opening Switch," IEEE Transactions on Plasma Science 21, 522 (1993).
9. P.G. Mikellides, A Theoretical Investigation of Magnetoplasmadynamic Thrusters, Ph. D. Dissertation Thesis, Ohio State University, 128 pages (1994).
10. P.G. Mikellides, P.J. Turchi, and N.F. Roderick, "Applied-Field Magnetoplasmadynamic Thrusters, Part 1: Numerical Simulations Using the MACH2 Code," Journal of Propulsion and Power 16, 887 (2000).
11. P.G. Mikellides and P.J. Turchi, "Applied-Field Magnetoplasmadynamic Thrusters, Part 2: Analytic Expressions for Thrust and Voltage," Journal of Propulsion and Power 16, 894 (2000).
12. P.G. Mikellides, P.J. Turchi, and N.F. Roderick, "Analysis of Applied-Field Plasma Thrusters Using the MACH2 Code," 1994, 1994).
13. P.G. Mikellides, P.J. Turchi, and N.F. Roderick, "Theoretical Model for Applied-Field MPD Thrusters," 31st AIAA/ASME/SAE/ASEE Joint Propulsion Conference and Exhibit (San Diego, CA, July 10-12, 1995, 1995).
14. Z.-G. Shen, C.-H. Liu, C.-H. Lee, C. Wu, and S. Yang, "A Study of a Coaxial Plasma Gun," Journal of Physics D: Applied Physics 28, 314 (1995).
15. K. Sankaran, E.Y. Choueiri, and S.C. Jardin, "Application of a new Numerical Solver to the Simulation of MPD Flows," 36th AIAA/ASME/SAE/ASEE Joint Propulsion Conference and Exhibit (Huntsville, AL, July 16-19, 2000, 2000).
16. M. Andrenucci, M. Caprili, and R. Lazzeretti, "Theoretical Models for Plasma Motion in Pulsed Coaxial Hydromagnetic Guns," 39th Meeting of the Advisory Group for Aerospace Research and Development Propulsion and Energetics Panel (USAF Academy, Colorado Springs, CO, June 12-15, 1972, 1972).).
17. T. Ao and T. Fujiwara, "Numerical and Experimental Study of an MPD Thruster," *17th International Electric Propulsion Conference* (Tokyo, Japan, 1984).
18. G.W.C. Kaye and T.H. Laby, *Tables of Physical and Chemical Constants, 10th edition* (Longmans, Green & Co., London, 1948)
19. S. Chapman, and T. G. Cowling, *The Mathematical Theory of Non-Uniform Gases*, Cambridge, University Press, 1960.
20. R. E. Peterkin, Jr., and M. H. Frese, *MACH: A Reference Manual-First Edition*, Air Force Research Lab, 1998.

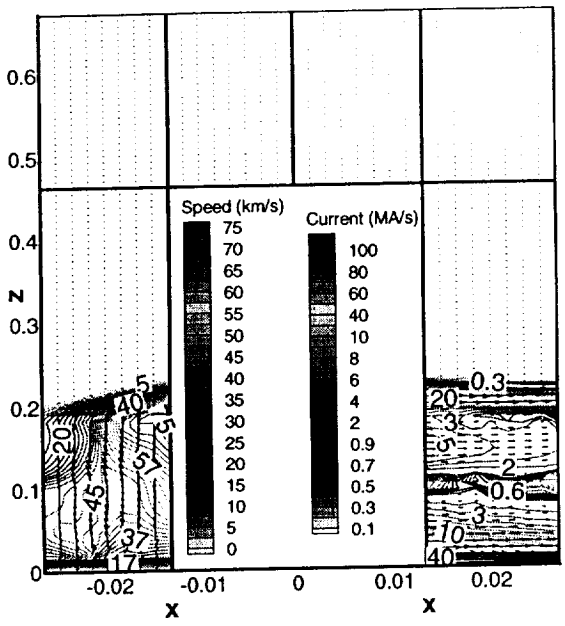

(a)

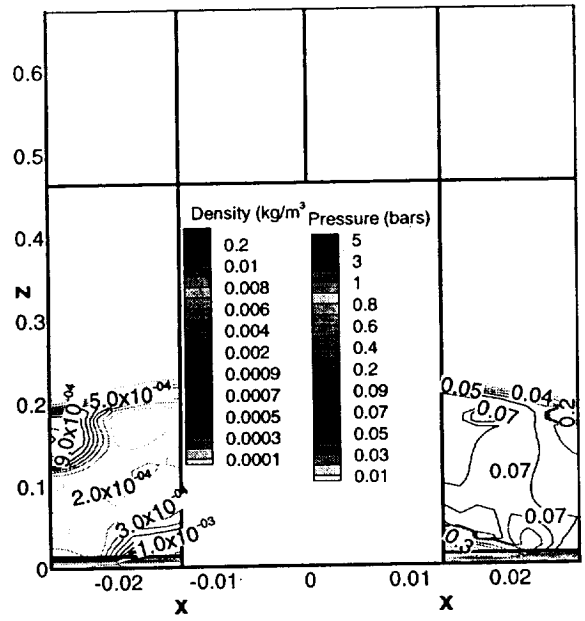

(a)

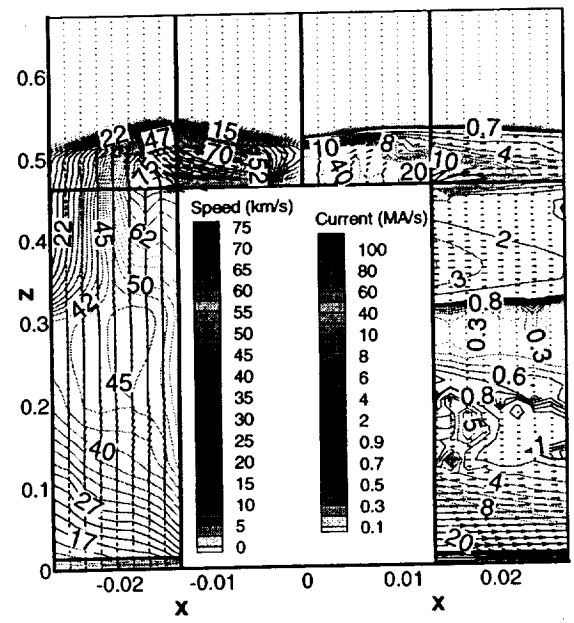

(b)

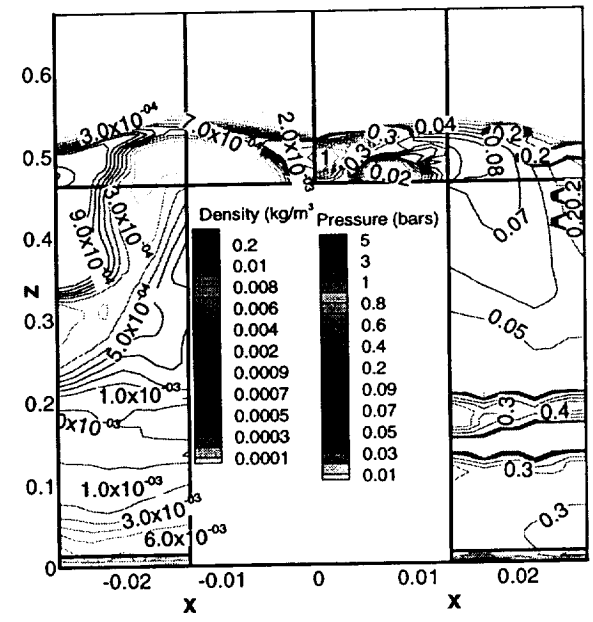

(b)

Figure 16. Mach 2 speed and current contours at (a) 7.5 μs and (b) 15 μs

Figure 17. Mach 2 density and pressure contours at (a) 7.5 μs and (b) 15 μs

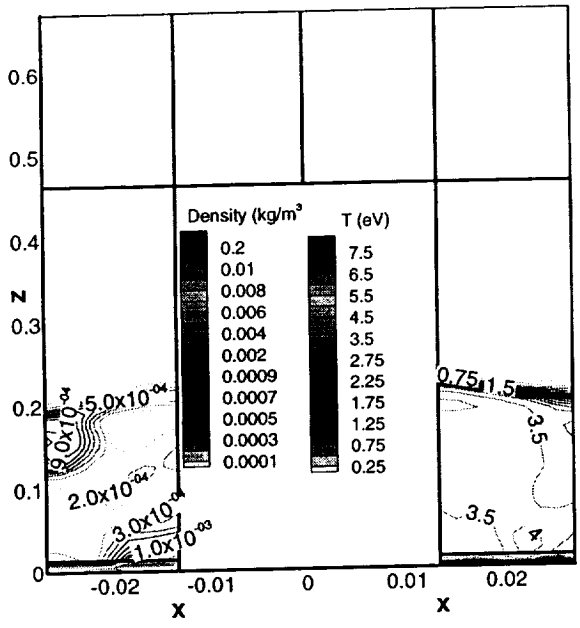

(a)

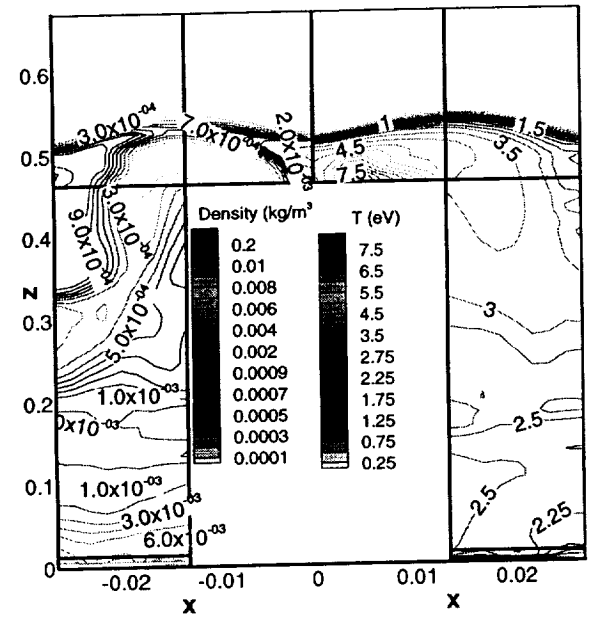

(b)

Figure 18. Mach 2 density and temperature contours at (a) 7.5 μs and (b) 15 μs